Acoustic waves and smart biomimetic nanoparticles: combination treatment from 2 to 3D colorectal cancer models

Cancer Nanotechnology

RESEARCH Open Access

Acoustic waves and smart biomimetic nanoparticles: combination treatment from 2D to 3D colorectal cancer models

Giada Rosso[1], Giulia Mesiano[1], Bianca Dumontel[1], Marco Carofiglio[1], Marzia Conte[1], Alessandro Grattoni[2,3,4] and Valentina Cauda[1*]

*Correspondence:
valentina.cauda@polito.it

[1] Department of Applied Science and Technology, Politecnico di Torino, C.So Duca Degli Abruzzi 24, 10129 Turin, Italy
[2] Department of Nanomedicine, Houston Methodist Research Institute, 6670 Bertner Ave, Houston, TX 77003, USA
[3] Department of Surgery, Houston Methodist Hospital, 6565 Fannin St., Houston, TX 77003, USA
[4] Department of Radiation Oncology, Houston Methodist Hospital, 6565 Fannin St., Houston, TX 77003, USA

Abstract

Colorectal Cancer (CRC) is the second leading cause of death among tumors worldwide. Conventional treatments are often accompanied by emerging immunotherapies, trying to reduce the burden of advanced and metastatic stages. Recently, nanomedicine therapies have been under intensive research to offer new perspectives to patients. Motivated by this rationale, this work proposes the formulation of advanced biomimetic and targeted nanoparticles (NPs) enabling a stimuli responsive and localized therapy, triggered by the safe use of acoustic shockwaves, a deep-penetrating tissue stimulation. Iron-doped zinc oxide nanocrystals were synthetized and enveloped in a biomimetic lipid bilayer shell, conjugating a peptide (YSA) as selective targeting toward CRC cells. Comparative studies, performed both in 2D monolayer and 3D spheroids of CRC models, between non-targeted (L-ZnO) and targeted (YSA-L-ZnO) nanoparticles demonstrated the superior capability of targeted nanosystems to dock and be internalized by CRC cells. The YSA-L-ZnO are proven to be highly biocompatible and hemocompatible, and capable of inducing selective damage, once activated by safe shockwaves. This mechanism is able to synergistically ablate tumor cells in both 2D and 3D models, proofing the concept of an innovative stimuli-responsive nanomedicine with a targeted and biomimetic strategy to offer future options for cancer fight.

Keywords: Zinc oxide nanocrystals, Lipid bilayer coatings, Shock waves, Targeting peptide, 3D cell spheroids

Graphical Abstract

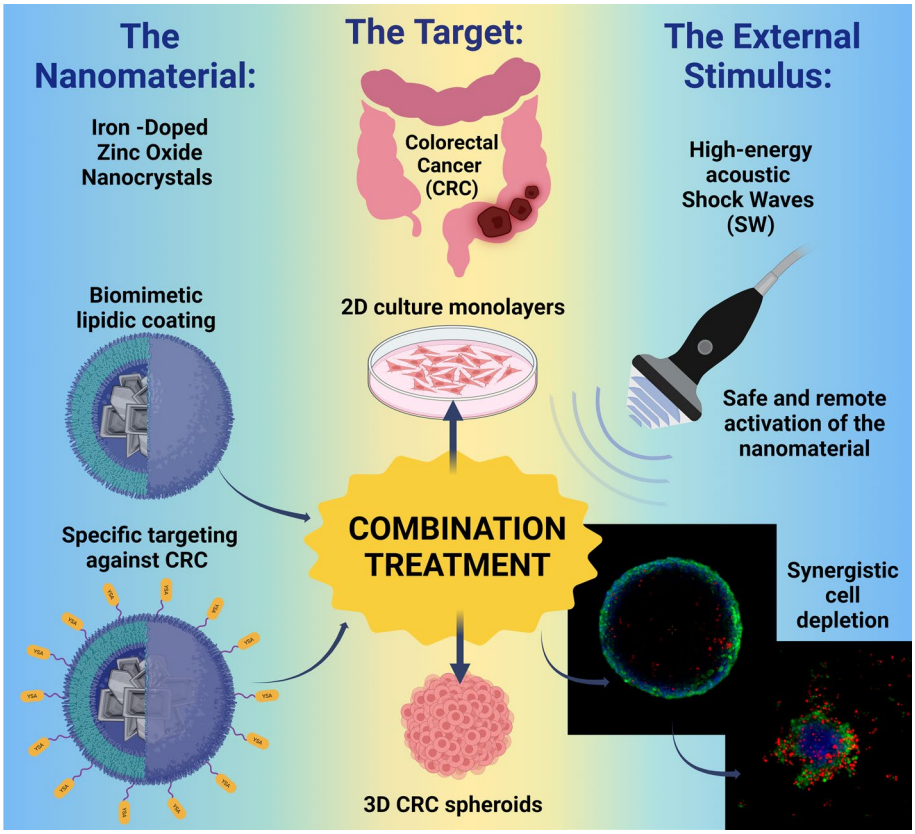

Background

According to the World Health Organization, Colorectal Cancer (CRC) is the third most diagnosed malignancy worldwide, representing approximately 10% of the totality of cancer cases (Sung et al. 2021) and the second cause of cancer-related demises. It is estimated that by 2040 the burden of CRC will exceed 3 million new cases each year. Nearly 25% of cases are diagnosed during advanced stages and metastatic CRC is still extremely lethal, showing a 5-year survival rate around 14% (Xie et al. 2020; Shin et al. 2023). Current treatments include surgery (predominant in the early stages), chemotherapy and radiotherapy, often administered in combination with immunotherapy in presence of metastatic lesions (Morris et al. 2023). Despite the emergence of both immune and targeted therapies (Xie et al. 2020), the greatest benefits for most CRC patients still come from chemotherapy combinations. However, chemotherapy drugs cause severe side effects, are often highly hydrophobic, with low biocompatibility and bioavailability at the tumor site and in 50% of cases they produce drug resistance and recurrent malignancies (Zhang et al. 2017; Sun et al. 2017).

Among the emerging technologies, possible innovative strategies against CRC could be offered by nanomedicine. The promise lies in having targeted nanoparticles (NPs) which can selectively affect malignant cells and the tumor microenvironment,

while sparing healthy tissues. Nanomedicine offers immense opportunities to play with nanomaterials, thus their interaction with biological environment can be tuned. However, there are still major challenges, almost unanimously recognized in: (i) obtaining biomimetic NPs, (ii) allowing smart and fully controllable functions, (iii) achieving a site-selective and timely targeted NPs to nullify off-target administration (Li et al. 2018; Sabu et al. 2018), (iv) address NPs administration and their capability to overcome the biological barriers to reach their target (Ouyang et al. 2023a, 2023b; Deng et al. 2024). In this respect, the strategy of developing biomimetic and high-performing therapeutic nanotools is valuable and can be accomplished by incorporating synthetic NPs into cell-derived (Ozsoy et al. 2024; Prasad et al. 2023, 2024a, 2024b; Zhang et al. 2022) or artificial lipid bilayers envelops (Percivalle et al. 2022; Conte et al. 2023). The role of biomimetics, once specifically referred to the biological identity of nanoparticles, is indeed to mimic natural mechanisms by combining synthetic and biological strategies to overcome the hurdles associated with the delivery of NPs in biological environment and prevent their recognition by the immune system and their consequent rapid clearance or premature degradation into potentially toxic by-products. Actually, cells use lipid bilayers as natural envelops, i.e. the cell membranes or extracellular vesicles. The amphiphilic chemical structure commonly shared by all classes of lipids is responsible for the formation of their characteristic bilayer arrangement in aqueous and biological environments. Therefore, they are considered good candidates for the stabilization of both organic and inorganic NPs, providing a defensive and biocompatible barrier (Luchini and Vitiello 2019), promoting a "safe" biological identity, stabilizing and improving the colloidal and chemical stability of inorganic nanoparticles in the biological environment (Percivalle et al. 2022; Dumontel et al. 2017).

Among inorganic NPs, zinc oxide nanocrystals (ZnO NCs) have already shown great potential application in vitro as well as in vivo for anticancer therapy due to their biocompatibility and pH-sensitivity, that assures effective endosomal drug release (Bisht and Rayamajhi 2016; Canta and Cauda 2020). Moreover, it has been recently demonstrated that iron-doped ZnO NCs (Fe:ZnO) present a higher biocompatibility towards both healthy and cancer cells, with respect to pristine ZnO (Carofiglio et al. 2020), possibly due to a reduced dissolution in potentially toxic Zn^{2+} ions (Xia et al. 2011). Furthermore, Fe:ZnO NCs show a magnetic behaviour, useful for future MRI detection, and enhanced responsiveness to energetic stimulation, like acoustic pressure waves, as previously demonstrated (Racca et al. 2023; Carofiglio et al. 2022).

The potentialities of NPs as therapeutic agent can be on-demand activated by energetic stimulation. When designing a therapy against cancer, deep tissue penetration and intrinsic safety of the used stimulus must be fulfilled. Acoustic pressure waves, like ultrasound and shock-waves (SW), have a broad application in medicine, from diagnostic echography to high intensity focused ultrasound (HIFU) with thermal effects for tumor thermoablation, or the most recent sonodynamic treatments, where acoustic waves are applied with sonosensitizers molecules or even NPs to treat cancer with non-thermal effects (Canavese et al. 2018). In a recent work of our group, the use of Fe:ZnO NCs in synergy with acoustic SW and in absence of released drugs was proposed as an effective strategy to treat CRC cells in vitro (Racca et al. 2023). This strategy opens perspectives

to on-demand activation of NPs with a harmless stimulus, without the risk of off-target release of a chemotherapeutic payload. As a step forward, in the present work, Fe:ZnO NCs have been equipped with a self-assembled phospholipidic coating, which can further improve their biocompatibility and colloidal stability in biological environment (Conte et al. 2023), and a targeting peptide for the active targeting of CRC malignant tissues.

In recent times, the emergence of 3D models has allowed cancer research to overcome some of the drawbacks linked not only to the use of 2D models, but also to in vivo murine ones (Breslin and O'Driscoll 2013; Costa et al. 2016). In addition to the ethical concerns, in vivo models are poorly representative and fail to mimic the complexity of the human body as they do not recapitulate the heterogenous tumor microenvironment and still differ from human activity in terms of metabolism and excretion (Searson 2023). To overcome such limitations, in vitro 3D models are a valuable tool to recapitulate various tumor features, contribute to the understanding of mechanisms of disease progression, identify pathways for therapeutic intervention and test new anticancer therapies (Searson 2023). Most importantly, key aspects such as cell–cell interplay and interactions with the extracellular matrix can be reproduced allowing for more precise human cancer pathobiology studies (Weiswald et al. 2015; Zanoni et al. 2016), as well as assessing the targeting and delivery of nanomedicines across endothelial and epithelial barriers (Searson 2023; Vakhshiteh et al. 2023) and penetration in 3D tumor (Tchoryk et al. 2019; Tian et al. 2021). These 3D models can thus greatly help to screen the NP therapeutic and targeting capabilities, while sparing animals, in accordance with 3Rs principles in animal experimentation (Replacement, Reduction and Refinement). Finally, both the FDA (Food and Drug Administration) (Han 2023) and the EMA (European Medicines Agency 2021) have recently published mandates highly recommending the use of 3D models as a valuable alternative to in vivo models.

Strategies that employ acoustic-wave stimulation and sonosensitizer drugs in 3D spheroid models have already been proposed (Roy et al. 2023; Foglietta et al. 2021; Leenhardt et al. 2019). Interestingly, polymeric NPs combined with drugs and acoustic stimulation were also successfully exploited in 3D settings for various cancer treatments (Li et al. 2019; Zhang et al. 2023; Wang et al. 2021). However, research strategies using biomimetic, targeted and stimuli-responsive NPs in absence of chemotherapeutics and exploring the potentialities of acoustic wave therapies have not yet been reported together.

Motivated by the above rationale, this study proposes the use of hybrid NPs, having a stimuli responsive hard core made of Fe:ZnO NCs and a biomimetic lipidic shell decorated with a targeting peptide (YSA) to enable a remotely controlled therapy by acoustic shock-waves in the complexity of 3D CRC models (Fig. 1).

After synthesizing and characterizing the YSA-L-ZnO, a comparison of their biocompatibility, hemocompatibility and targeting selectivity with non-targeted L-ZnO NPs is proposed in 2D cell culture of CRC tumor cells and healthy counterpart and then in a 3D tumor model. Furthermore, the evaluation of the NPs safety profile and ability to kill cancer cell models upon acoustically triggered activation is presented. The results show that YSA-L-NPs are fully safe at the dose utilized in the treatments and can become highly cytotoxic on demand, once stimulated with SW.

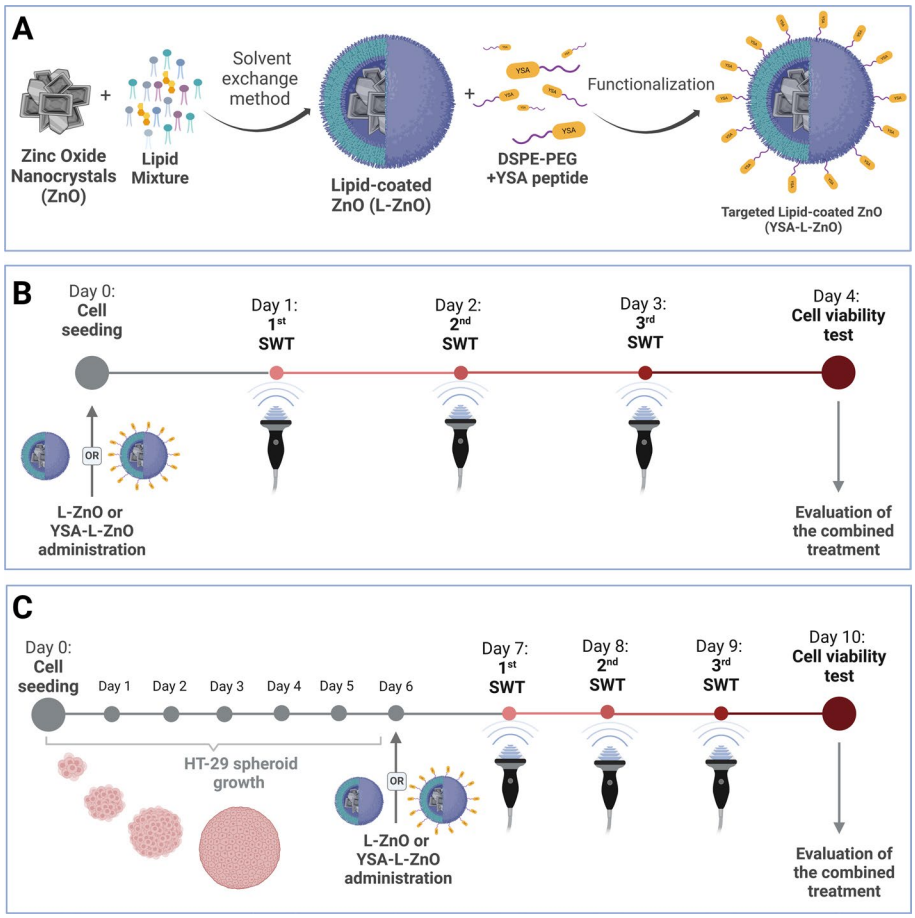

Fig. 1 Scheme of the proposed NPs and stimuli-responsive treatment. **A** Preparation of the biomimetic nanoparticles: ZnO nanocrystals were synthesized, coated with a self-assembling lipid formulation (L-ZnO), adopting a solvent-exchange method, and then conjugated with the targeting peptide (YSA) bound to a functional lipid (Conte et al. 2023; Cauda et al. 2010); **B** Experimental setting of the stimuli-responsive therapy for 2D monolayer setting of CRC cells (HT-29 cell line): cells were seeded and administered with L-ZnO or YSA-L-ZnO the first day, then at 24, 48 and 72 h they were subjected to multiple shock waves treatments (SWT) and their viability was evaluated 96 h after cell seeding; C) Experimental setting in 3D spheroids of CRC (HT-29 cell line). Cells were seeded and left to grow for 6 days; at day 6, the spheroids received the L-ZnO or the YSA-L-ZnO treatment. Then, at days 7, 8 and 9, they were subjected to multiple shock waves treatments (SWT); finally, the spheroid viability was evaluated at day 10

The proposed combination therapy, realizing a synergistic treatment with a deep penetrating and harmless stimulus, is an innovative nanomedicine strategy to potentially offer valuable options in future for cancer fight.

Experimental section

Nanoparticle synthesis

Iron-doped zinc oxide nanocrystals (here simply referred to as ZnO) were synthetized following a previously reported method (Carofiglio et al. 2021). Briefly, 526 mg of zinc acetate dihydrate ($Zn(CH_3COO)_2{\cdot}2H_2O$, Sigma-Aldrich) and 58 mg of ferric nitrate hexahydrate ($Fe(NO_3)_3{\cdot}9H_2O$, HiMedia), corresponding to 6%mol of doping, were dissolved in 40 mL of absolute ethanol (99%, Sigma-Aldrich) in a round bottom flask. The solution

was heated to 70 °C and stirred until complete dissolution of zinc and iron precursors. Additionally, 140 µL of oleic acid capping agent (≥ 99%, Sigma-Aldrich) and 1 mL of bidistilled water (obtained from a Direct Q3 system, Millipore) were added.

Separately, 1.044 g of tetramethylammonium hydroxide pentahydrate (TMAH, 98.5%, Sigma-Aldrich) were dissolved in 10 mL of ethanol and 1.052 mL of water. The TMAH solution was rapidly poured in the precursors solution to initiate particle condensation and the reaction was carried out under continuous stirring at 70 °C for 10 min. Then, 40 mL of ice-cooled ethanol were added to the solution to arrest the reaction. The resulting colloidal solution was collected and centrifuged at 8000 g for 10 min and washed three times with fresh ethanol. The obtained ZnO NPs were further functionalized with amino groups to successively enable the attachment of dyes for in vitro applications. In detail, 40 mg of synthesized ZnO were suspended in ethanol at a concentration of 2.5 mg/mL. The solution was heated to 70 °C with moderate stirring under reflux conditions and nitrogen atmosphere. Subsequently, 8.6 µL of (3-Aminopropyl) trimethoxysilane (APTMS, Sigma-Aldrich), equal to 10%mol of ZnO, were added. The NPs dispersion was left under moderate stirring in an inert atmosphere for 6 h. At the end of the reaction time, the dispersion was collected and centrifuged at 12,000 g for 20 min. The supernatant was discarded, and the particles were washed twice and then resuspended in 10 mL of ethanol.

NPs coating with lipid bilayer and conjugation with targeting peptide

To obtain a stable coating, a previously developed protocol was employed (Conte et al. 2023), consisting in a solvent exchange method which also exploits an electrostatic interaction between the ZnO and the lipid mixture. The latter in fact includes an anionic phospholipid, DOPA (18:1 PA, 1,2-dioleoyl-sn-glycero-3-phosphate (sodium salt, chloroform solution), which is believed to interact with the positively charged surface of the aminopropyl-functionalized ZnO. Briefly, a lipid mixture composed by DOPA, DOPC (18:1 (Δ9-Cis) PC (DOPC), 1,2-dioleoyl-sn-glycero-3-phosphocholine, chloroform solution) and DSPE-PEG (2000) Amine (1,2-distearoyl-sn-glycero-3-phosphoethanolamine-N-[amino(polyethylene glycol)-2000] (ammonium salt)) from Avanti Polar Lipids and cholesterol in chloroform solution from Sigma-Merk was prepared with 50:10:1.5:38.5 molar ratio. The solution, placed in a glass vial, was left to dry under vacuum overnight and rehydrated with a mixture of ethanol and water, obtaining a 3 mg/mL final concentration, respecting an ethanol:water volume ratio of 2:3. NPs to coat were then collected from the ethanolic stock suspension and pelleted through centrifugation at 14,000 g for 10 min. Supernatant was discarded and the lipid mixture was added, following a lipid:ZnO weight ratio of 1:2. The obtained suspension was sonicated for 3 min at 59 kHz in an ultrasound bath (Branson 3800 CPXH) and b.d. water was quickly added to obtain an abrupt solvent exchange able to drive the self-assembly of the phospholipids around the ZnO. The final concentration of the so obtained lipid coated ZnO (L-ZnO) was set to 1 mg/mL and additional sonication of 5 min was applied to homogenize the sample.

Similarly, YSA-targeted nanoconstructs (YSA-L-ZnO) were obtained by adding to the lipid mixture, prior to vacuum-drying, 0.3% molar of DSPE-PEG (2000)-Maleimide (1,2-distearoyl-sn-glycero-3-phosphoethanolamine-N-[maleimide(polyethylene glycol)-2000]

(ammonium salt)) from Avanti Polar, pre-conjugated with the targeting ligand. Such binding was obtained, as reported by Conte et al. (2023), incubating the PEGylated phospholipid, once dried and resuspended in Dimethylformamide (DMF, Sigma-Aldrich) at a concentration of 37.5 mM, with the peptide solution for 1 h at room temperature. The peptide, whose whole sequence is YSAYPDSVPMMS (prepared by Bio-Fab Research srl, Rome, Italy), was designed to bind to the Epha2 receptor, overexpressed by HT-29 cells, as reported in a previous work (Koolpe et al. 2002), but modified by adding a cysteine aminoacid to conjugate with the maleimide group exposed by the PEGylated lipid. The peptide solution was prepared by adding DMF, reaching 50 mM peptide concentration and successively diluted with 0.1 M PBS (pH = 7.4), achieving 10 mM final concentration. The lipid solution is added to the obtained mixture following a 3:1 phospholipid:peptide molar ratio and stored, after incubation, at − 20 °C until utilization (Barui et al. 2022, 2023; Schnorenberg et al. 2018).

NPs characterization

To assess the appearance of the final nanoconstruct, the lipid-coated nanoparticles dispersed in bidistilled water were vitrified and imaged at the Baylor College of Medicine Cryo-Electron Microscopy Core Facility (Texas Medical Center, Houston, TX). Vitrified Quantifoil R1.2/1.3 300Cu (Quantifoil Micro Tools GmbH, Jena, Germany) grids were imaged with a Thermo Fisher Glacios Electron Microscope (Thermo Fisher Scientific Inc) operating at 200 kV. Field emission scanning electron microscopy (FESEM) images were acquired with a Supra 40 from Zeiss. The sample was prepared by depositing 10 μL of ethanolic NPs stock solution directly onto a monocrystalline silicon substrate. The NPs X-ray diffraction pattern was acquired with a Panalytical X'Pert diffractometer working in Bragg–Brentano mode (Cu Kα source, λ = 0.154 nm, 30 mA and 40 kV) on similarly prepared samples.

In order to evaluate the correct assembly of the L-ZnO and YSA-L-ZnO nanoconstructs, the hydrodynamic radius and the Zeta potential were measured through Dynamic Light Scattering (DLS), employing a Zetasizer Nano ZS90 (Malvern Panalytical), before and after the lipid coating through solvent exchange method. The measurements were performed in bidistilled water, or in RPMI 1640 cell culture media, dispersing NPs at a concentration of 100 μg/mL.

Fluorescence microscopy was also performed on YSA-L-ZnO, to have a qualitative idea of the presence of the targeting peptide on NPs surface. Prior to the lipid coating step, the NPs were labelled with ATTO 550-NHS ester (Thermofisher) by adding 2 μL of the dye (2 mg/mL in DMF) per mg of NPs, resuspended in ethanol at a concentration of 1 mg/mL. The particles were stirred overnight, protected from light, to let the dye bind to the aminopropyl group of the NPs surface functionalization. After two washings steps consisting in centrifugation at 14,000 g for 10 min and substitution of the supernatant with fresh ethanol, the particles were coated with the lipid bilayer as descripted above, but using a FITC-labelled YSA peptide (from Bio-Fab Research srl). A little drop of diluted sample was deposited on a glass slide and analysed through spinning disk confocal microscopy (Ti2 Nikon equipped with a crest large FOV laser and a 100 × PlanAPO objective, NA = 1.30). At least 10 images per sample were analysed with the colocalization tool of the NIS software from Nikon.

Hemocompatibility assays

Lipid bilayers should confer to the NPs superior biocompatibility, of which an essential aspect is hemocompatibility. To assess if L-ZnO and YSA-L-ZnO possess increased hemocompatibility, a plasma recalcification test was performed. Uncoated and coated NPs were resuspended in physiological solution, at a concentration of 100 or 200 μg/mL. A 96-well plate was filled adding in each well 75 μL of human citrated plasma (Human Recovered Plasma Pooled- frozen—Na Citrate from ZenBio), pre-heated at 37 °C. Afterwards, 75 μL of each sample was added in the plate, at least in 6 wells, obtaining a final concentration of the NPs equal to 50 and 100 μg/mL. The plate was then incubated at 37 °C for 5 min, and immediately after, 150 μL of 25 mM $CaCl_2$ water solution (pre-heated at 37 °C) were quickly added to half of the wells and the plate was immediately inserted in the plate reader (pre-heated at 37 °C) of a Multiskan GO microplate spectrophotometer (Thermo Fisher Scientific). The absorbance of the samples in the UV–Vis range was measured at 405 nm every 30 s for a period of 45 min at 37 °C, evaluating the coagulation of plasma over time. Three independent experiments were performed and for each one the coagulation time of every sample was calculated as the mean of the time points corresponding to the flex of the sigmoid curve, produced by the evolution of absorbance of the coagulating samples, as previously reported (Cauda et al. 2021).

2D in vitro cytotoxicity test

The cytocompatibility of L-ZnO and YSA-L-ZnO was initially assessed in conventional 2D cultures of CRC HT-29 and its healthy counterpart, CCD18-CO cell lines (product CRL-1459 from ATCC). HT-29 cell line was maintained in RPMI 1640 medium (ATCC) supplemented with 10% FBS (ATCC) and 1% of 100 μg/mL of streptomycin/100 units/mL of penicillin (P/S, Sigma-Aldrich). CCD-18CO cell line was instead cultured in Stable Cell MEM (Sigma) supplemented with 10% FBS, 1% P/S, 1% MEM, 1% L-Glut and 1% sodium pyruvate. The cytotoxicity test was performed by seeding, in a 96 well plate (TC Treated, Thermo Fisher) 5000 cells/well (HT-29) or 10,000 cells/well (CCD-18CO) in 100 μL of cell culture medium, in which L-ZnO or YSA-L-ZnO were dispersed at different concentrations: 0, 15, 30, 50, 75 and 100 μg/mL. 24, 48, 72 and 96 h after seeding, the viability of cells was evaluated through the WST-1 metabolic colorimetric assay. 10 μL of WST-1 reagent (Roche) were added in each well; the plate was incubated for 2 h and then inserted in a plate reader (Multiskan GO microplate spectrophotometer, Thermo Fisher Scientific) to measure the absorbance at 450 nm and 620 nm. The absorbance at 620 (reference) was subtracted to the one at 450 and the obtained signal, once removed the background, was normalized according to the non-treated sample, which was set to 100% viability.

2D nanoparticles uptake evaluation

To estimate the ability of the nanoconstructs of being internalized by cells, cells were seeded in a 24-well plate (TC Treated, Thermo Fisher) at a concentration of 5×10^4 cells/well (HT-29) or 10×10^4 cells/well (CCD-18CO) in 500 μL of cell culture medium, in which 0 (non-treated control), 30 or 50 μg/mL of L-ZnO or YSA-L-ZnO, previously labelled with the lipophilic dye DiD (Thermofisher) were added. To label the lipidic shell, 5 μL of DiD (10 μg/mL stock in DMSO) were added for each mg of NPs; successively the

NPs were incubated in a shaker at 37 °C, 250 rpm for 30 min. 2, 5, 24 and 48 h after the seeding of the cells, the uptake of L-ZnO and YSA-L-ZnO was evaluated through flow cytometry. In brief, cells were washed with PBS and trypsinized. Then, the collected cells were washed twice in PBS by centrifugation (130 g, 5 min) and successively dispersed in 250 µL PBS. The obtained suspension was analysed with a flow cytometer (Guava easyCyte 6-2L flow cytometer by Merck Millipore).

The fluorescence microscopy images were taken with spinning disk confocal microscopy (Ti2 Nikon equipped with a crest large FOV laser and a 100 × PlanAPO objective, NA = 1.30). Cells were treated with fluorescently labelled L-ZnO or YSA-L-ZnO, while ZnO cores were labelled with ATTO 550-NHS, as above, and the lipidic shell by adding 1 µL of a lipophilic dye DiO (1 mg/mL solution in Dimethyl sulfoxide, Thermofisher) for each mg of ZnO, while cells membrane were stained with 24 µg /mL of WGA-647 and cell nuclei with 6 µg/mL Hoechst.

2D stimuli-responsive NPs treatment

To evaluate the effect of the combined treatment, HT-29 or CCD-18Co cells were seeded in a 96 well plate, as for the cytotoxicity tests, but leaving at least one empty well in each direction between seeded wells, to avoid influence of the SW treatment to the surrounding wells. Cells were left untreated or treated with 30 or 50 µg/mL of L-ZnO or YSA-L-ZnO. After 24, 48 and 72 h from the administration of the NPs, half of the wells were subjected to a shockwave treatment, administered with a Piezowave, PW^2 (Richard Wolf, ELvation Medical device), stimulating the plates from the bottom by positioning the transducer covered with ultrasound gel (Stosswellen Gel, ELvation Medical GmbH) in correspondence to the well to treat as described elsewhere (Racca et al. 2023). Each SW administration consists in 250 shots of high-energy focalized shockwaves at 4 shots/s, at E6 or E9 energy levels, corresponding to 0.22 or 0.35 mJ/mm^2, respectively. 96 h after cell seeding, viability was evaluated through WST-1 assay, as above.

Cytotoxicity, NPs uptake tests and stimuli-responsive NPs treatment on 3D cell cultures

To obtain HT-29 spheroids, 10×10^3 cells/well were seeded in a round bottom-ultra low attachment 96-well plate (Corning) with 100 µL of culture medium. The plate was centrifuged at 250 g for 5 min and the spheroids were left to grow for 6 days, adding 50 µL of fresh medium every 3 days. To assess the cytotoxicity of the NPs in the 3D cultures, at day 6, the spheroids were transferred to a regular 96-well plate (suspension, Greiner Bio-One), together with 50 µL of their original medium. Thereafter, other 50 µL of fresh medium with or without the NPs were added to each well, in order to obtain a final concentration of 50, 75 and 100 µg/mL of L-ZnO or YSA-L-ZnO. 24, 48, 72 and 96 h after the treatment with NPs, the viability of the spheroids was assessed through flow cytometry. At least three spheroids per condition were collected and put together in an Eppendorf tube and washed two times with PBS, by means of centrifugation at 130 g for 5 min. Afterwards, 50 µL of Accutase (Sigma-Aldrich) were added to disaggregate the spheroids. After 30 min of incubation at 37 °C, the spheroids were washed again two times in PBS, and resuspended in a final PBS solution containing 1 µL/mL of Propidium Iodine (PI, ThermoFisher) to label dead cells.

Similarly, to evaluate the internalization of the NPs in the 3D HT-29 culture, at day 6 after seeding, the spheroids were treated with 75 or 100 µg/mL of L-ZnO or YSA-L-ZnO, precedingly labelled with DiD. The level of internalization was assessed through flow cytometry, at 24, 48 and 72 h after the treatment.

Along the lines of the above tests, the effect of the combined treatment was also evaluated. At day 6 after seeding, the spheroids were treated with 75 or 100 µg/mL of L-ZnO or YSA-L-ZnO and 24, 48, 72 after, a SW treatment was administered as described before (each consisting in 250 shots at E6 or E9 energy level). 96 h after the treatment with NPs, the viability of the spheroids was assessed through flow cytometry, thanks to the addition of PI.

Spheroids treated and disaggregated in the same way were employed to evaluate the level of apoptosis. To detect the apoptotic cells, Guava Nexin Reagent (Lumiex) kit was used, following the manufacturer's instructions.

Spheroids fluorescence microscopy

Cells in the spheroids were stained by directly adding the fluorescent dyes in the culture media, followed by 30 min incubation at 37 °C. Nuclei were labelled with Hoechst, (6 µg/mL), live cells with Calcein AM (1 µl/mL of 2 mM stock solution) and dead cells with Propidium iodine, (2 µg/mL). The spheroids were analysed through spinning disk confocal microscopy (Ti2 Nikon equipped with a crest large FOV laser and a 100 × PlanAPO objective, NA = 1.30), performing a Z-stack to allow the reconstruction through NIS software from Nikon of the spheroids volume.

Statistical and synergy analysis

All the presented biological tests were carried out at least in triplicate and Two-Ways ANOVA tests were performed with GraphPad Prism 9; $^{*}p < 0.0332$, $^{**}p < 0.0021$, $^{***}p < 0.0002$, $^{****}p < 0.0001$. Synergy scores were obtained through SynergyFinder^{+} (SynergyFinder—a FAIR tool for drug combination discovery), a free web-application for interactive analysis. The data were obtained providing, as input of the analysis tool, the results of the viability tests collected after the combination treatment with shock waves. To calculate the Synergy score, the Highest Single Agent (HSA) model was employed (Ianevski et al. 2022). The resulting score is based on the deviation from the expected and the obtained responses to the combination of two or more treatments. This combination can be either synergistic (synergy score > 10), when the obtained effect is higher than the expected one, or antagonistic (synergy score < − 10), when the effect is lower than the expected. If the synergy score is between − 10 and 10, the obtained effect is in line with the expected one and the interaction is additive.

Figures

All the graphs were created in GraphPad Prism 9 and all the schemes were produced with BioRender.com.

Results and discussion

Biomimetic NPs preparation

Iron-doped zinc oxide nanocrystals, for simplicity referred hereinafter as ZnO, were synthesized by a wet chemistry method and then chemically functionalized at their surface with amino-propyl groups. As previously optimized (Carofiglio et al. 2021), oleic acid, a common capping agent for the production of monodisperse and uniform NPs, was used and iron doping was assessed of 6% At to avoid the formation of a separate phase. The introduction of iron doping to ZnO has been shown to guarantee better biocompatibility in cell cultures (Xia et al. 2011; Carofiglio et al. 2022; George et al. 2010) and to attribute additional magnetic properties (Carofiglio et al. 2021), which could be exploited for theranostic scopes in future works.

The synthesized nanocrystals presented an almost spherical shape of around 10 nm of diameter and a crystalline wurtzitic phase as shown by the FESEM image and X-ray diffraction pattern reported in Figure S1A and Figure S1B of Supporting Information (S.I.), respectively.

In order to stabilize the nanocrystals in biological environment and thus increase the bio- and hemocompatibility of the ZnO as well as to accomplish biomimetics and colloidal biostability, a phospholipidic coating composed by regular and anionic phospholipids, cholesterol and PEGylated phospholipids was formulated, based on previous seminal works of our group (Conte et al. 2023; Dumontel et al. 2017; Rosso and Cauda 2023). Furthermore, PEGylated phospholipids were exploited to build a functional lipid conjugating the ephrin-mimetic peptide YSA, specifically targeting the EphrinA2 (EphA2) receptor (Koolpe et al. 2002). The high expression of EphA2 receptor by CRC cell line is well recognized in the literature (The human protein Atlas) and was confirmed by Western Blot analysis in the HT-29 CRC cell line employed in this study (Figure S2 of the S.I.).

ZnO NCs were coated by lipids exploiting a solvent exchange method (Conte et al. 2023; Cauda et al. 2010): owing to the electrostatic interaction among the positively charged nanocrystals and the mainly negatively charged lipid mixture, the lipids easily self-assemble upon hydration forming a thin bilayer around clusters of nanocrystals, as visible through Cryogenic electron microscopy (CryoEM) (Fig. 2A). The effectiveness of the coating is evidenced with respect to uncoated ZnO (average hydrodynamic size: 120 nm, Polydispersity Index (PdI): 0.096 as depicted in the black curve in Fig. 2B**)** by an increase of the hydrodynamic size in water of L-ZnO and YSA-L-ZnO (Fig. 2B), which measures 185.2 nm (PdI = 0.23) and 207.7 nm (PdI = 0.28), respectively, and by the shift in the Zeta potential values from positive to negative (Fig. 2D). Despite not being in the conventional monodispersity range (PdI < 0.1), the PdI of the lipid-coated ZnO is in the moderate polydispersity range (PdI < 0.4), and the values obtained are still acceptable in lipid-based drug delivery systems (Danaei et al. 2018). The single peak of the size distributions further confirms the overall quality of the lipid-coated samples. DLS measurements were also performed in cell culture medium (Fig. 2C), testifying a good stability of the lipid-coated ZnO, which show results comparable to the ones obtained in water (L-ZnO: 172.73 nm, PdI = 0.30 and YSA-L-ZnO: 204.2 nm, PdI = 0.21). In contrast, pristine ZnO manifest an increase of size (194.8 nm, PdI = 0.31, which suggests a tendency to aggregate in biological environments. To assess the presence of the targeting

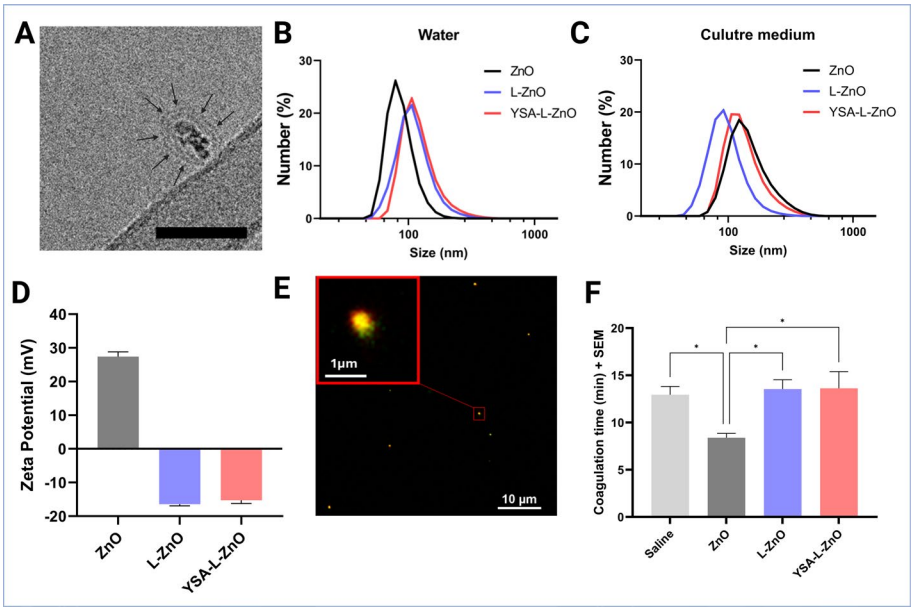

Fig. 2 **A** Cryo-Electron Microscopy (CryoEM) image of lipid-coated Zinc Oxide Nanocrystals (L-ZnO), depicting the ZnO nanocrystals surrounded by a visible lipid bilayer, evidenced by the black arrows. Scale bar is 50 nm. **B** Dynamic Light Scattering (DLS) of uncoated (ZnO) and lipid-coated (L-ZnO, YSA-L-ZnO) in water and **C** in cell culture media; **D** Z-Potential of uncoated (ZnO) and coated (L-ZnO, YSA-L-ZnO) in water; **E** Spinning disk confocal fluorescence microscopy image of YSA-L-ZnO, where ZnO and YSA peptide were fluorescently labelled with Atto550 and FITC dyes, respectively, thus visible as red and green signals; **F** Hemocompatibility studies comparing the clotting time of human plasma after calcium chloride addition in absence and in presence of ZnO, L-ZnO or YSA-L-ZnO

peptide on the nanoconstruct, a fluorescently labelled peptide was conjugated with the phospholipids and assembled on labelled nanoparticles. The obtained YSA-L-ZnO were investigated through confocal fluorescence microscopy, observing a high colocalization of the two fluorescent elements ($87.3 \pm 11.4\%$,) indicating the compresence of ZnO NCs and YSA peptide bound to the lipidic shell in the majority of cases (Fig. 2E).

Additionally, uncoated and lipid-coated ZnO were tested on human plasma citrate for an in vitro recalcification test (Fig. 2F) (Cauda et al. 2021; Tavano et al. 2010), evidencing an excellent hemocompatibility of L-ZnO and YSA-L-ZnO. For both samples the coagulation times were comparable to the physiological solution in plasma. On the contrary, pristine ZnO produced an earlier coagulation of the plasma; this indirectly demonstrates the correct assembly of the lipids around the nanocrystals and their role in isolating the ZnO core from the biological environment.

In vitro test of nanoparticles in cell cultured monolayers

2D cytotoxicity test

Firstly, the cytotoxicity of L-ZnO and their targeted counterpart, YSA-L-ZnO, was evaluated on HT-29 CRC cell line and on CCD-18Co, a cell line exhibiting fibroblast morphology that was isolated from the normal colon tissue. The main goal of this preliminary assay was to find the optimal doses of NPs for cell treatment that can influence the viability of HT-29 cells, but without substantially damaging them, while sparing the

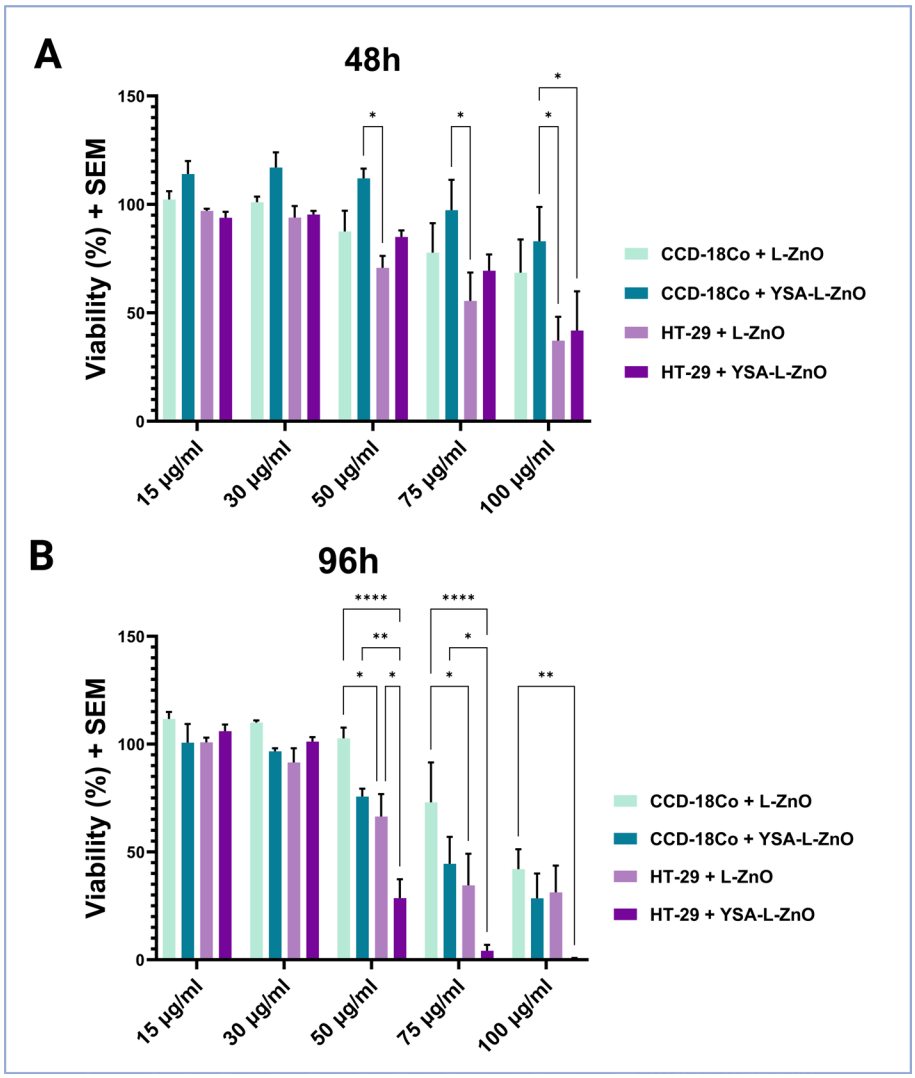

Fig. 3 Cytotoxicity test on monolayer cultures of HT-29 CRC malignant cells and CCD-18Co fibroblast-like, healthy colorectal cells. Cells were treated with different concentrations of L-ZnO and YSA-L-ZnO (15, 3, 50, 75 and 100 µg/mL). Cell viability was measured trough WST-1 metabolic assay after cells exposure to the nanoparticles. Data are expressed as normalized percentage with respect to the control sample, which was considered 100% viable. *$p < 0.0332$, **$p < 0.0021$, ***$p < 0.0002$, ****$p < 0.0001$

healthy counterpart. The choice of the correct dose is in fact crucial, since this work aims at a safe-by-design nanoconstruct, that uses a subtoxic NP concentration in view of the further combination with the acoustic stimulation for exclusive depletion of cancer cells.

The viability of HT-29 and CCD-18Co was assessed at 24, 48, 72 and 96 h after administration (i.e. at day 1, 2, 3 and 4 of the treatment as depicted in the scheme of Fig. 1B) and the results, presented in Fig. 3 and Figure S3, clearly indicate a very high biocompatibility of both L-ZnO and YSA-L-ZnO NPs up to 50 µg/mL in both cell lines. At 50 µg/mL and above, a strong dose- and time-dependent toxicity was observed in HT-29 cells after 48 h from administration (Fig. 3A). Remarkably, CCD-18Co healthy cells were less affected by the nanoconstructs and at 48 h, a statistically significant difference between the two cell lines was observed, evidencing a higher cytotoxicity on HT-29 cells. At 96 h

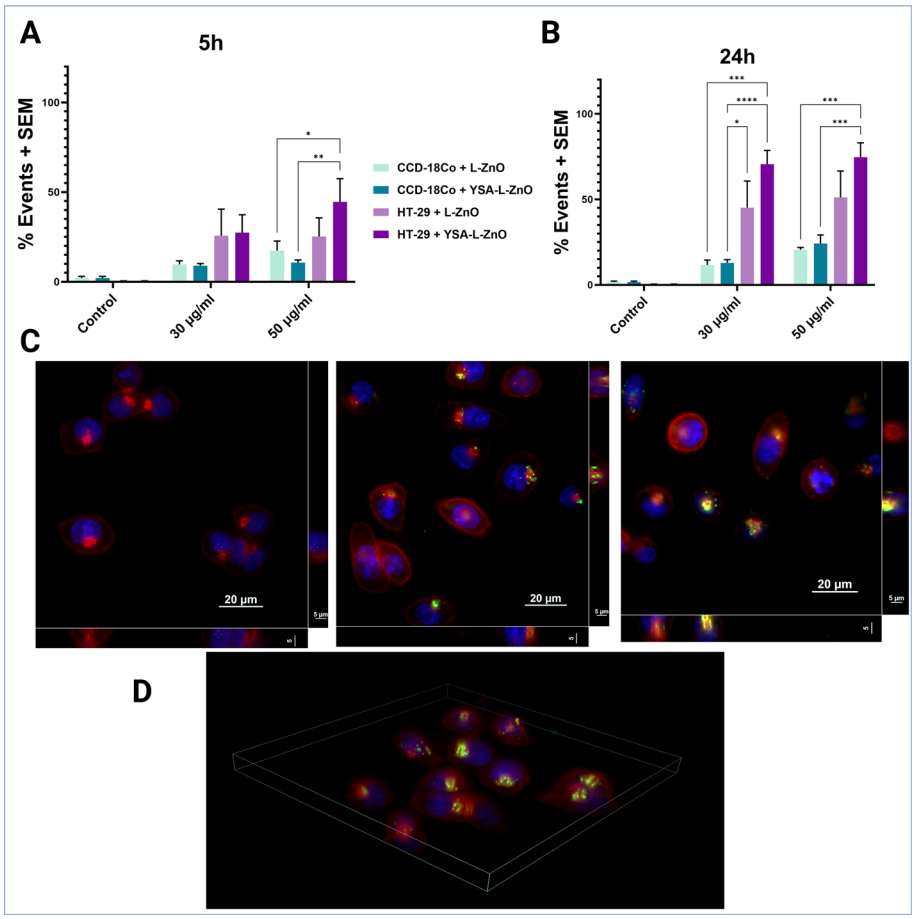

Fig. 4 Flow cytometry results of nanoparticles internalization tests onCCD-18Co fibroblast-like, healthy colorectal cells and HT-29 CRC malignant cells at **A**) 5 h and **B**) 24 h after NPs treatment. **C** Spinning disk fluorescence microscopy of HT-29 cells untreated (Control) or treated with L-ZnO or YSA-ZnO. Multiple images were taken for each sample, to obtain a Z-stack; the projection of the 3D reconstructed image is visible in the right and bottom part of each panel. Nuclei were stained with Hoechst (blue) and cell membrane with WGA-647 (red). ZnO cores were stained with ATTO-550 (yellow) and the lipidic shell were labelled with DiO (green). **D** Reconstructed fluorescence microscopy 3D image of HT-29 cells treated with YSA-L-ZnO. *$p < 0.0332$, **$p < 0.0021$, ***$p < 0.0002$, ****$p < 0.0001$

post administration, (Fig. 3B), this trend resulted strengthened and a severe toxicity was produced in HT-29 cells at the highest concentrations, especially if treated with YSA-L-ZnO, demonstrating the strongest effect of the targeted NPs on this cell line. For this reason, 30 and 50 µg/mL NPs concentrations were chosen as the optimal doses for the following SWT experiments, being the highest biocompatible doses on both healthy and cancer cell lines, in view of the further addition of the SW treatment.

Nanoparticles uptake and targeting ability in 2D cell cultures

To assess the efficacy of the YSA peptide in targeting CRC cells, an uptake experiment was set up, comparing the cell internalization of fluorescently labelled L-ZnO and YSA-L-ZnO in both tumoral and healthy cell lines by flow cytometry (Fig. 4 and Figure S4). In the case of HT-29, the data demonstrate a time-dependent uptake, which tends to

considerably increase, in the first 24 h after NPs administration, and shows statistically significant differences with respect to the healthy cell line already at 5 h post administration (Fig. 4A). Remarkably, this behaviour resulted enhanced at 24 h (Fig. 4B), when the difference between the two cell lines is substantial. Notably, a higher uptake of YSA-L-ZnO than L-ZnO was observed and this happened only in the HT-29 cancer cell line, with a difference of approximately 15% in positive events between targeted vs untargeted NPs. A completely different behaviour was observed for CCD-18Co cell line: the percentage of positive events remains quite stable in time, never exceeding 40% even at the highest doses. Furthermore, no preferential internalization was observed for the YSA-L-ZnO with respect to the L-ZnO. The collected data indicate that YSA peptide plays an important role in the interaction between nanoparticles and HT-29 cell membranes, proving that this peptide is a good candidate for the selective targeting of CRC cells.

To obtain some visual insights and a qualitative evaluation of the cell internalization, HT-29 cells were treated with fluorescently labelled L-ZnO or YSA-L-ZnO and analysed through confocal microscopy 24 h post administration. Figure 4C shows the untreated control cells (left panel), cell treated with L-ZnO (central panel) and YSA-L-ZnO (right panel) where the stained cell membranes are visible in red, the nuclei in blue, the lipidic shell of the nanoconstructs in green and the ZnO core in yellow. Finally, Fig. 4D is a representative 3D reconstructed image of HT-29 cells treated with YSA-L-ZnO. All together these data evidence that the NPs are readily internalized by cells, ending up in the perinuclear cytoplasm area.

Acoustic stimuli-responsive treatment of 2D cell cultures

With the aim of evaluating the effect of the combination treatment, acoustic stimuli consisting in repeated and intense pressure impulses, i.e. acoustic shock waves (SWs), were administered to NPs-treated CCD18-Co and HT-29 cells. SWs were produced by the PiezoWave (PW^2) device by Elvation Medical, which is currently employed in clinics for treating muscle-skeletal diseases (PiezoWave2 E eswt/piezowave^2/), and was repurposed in this work against CRC. Based on our previous studies (Racca et al. 2023), which demonstrated the effectiveness of repeated SW treatments (SWT), three consecutive SWT were administered at 24, 48 and 72 h from NPs administration (as depicted in Fig. 1B). Two different intensities of SWs were tested: energy levels E6 and E9, corresponding to 0.22 mJ/mm^2 and 0.35 mJ/mm^2, respectively; the results are presented in Fig. 5A and Figure S5.

E6 energy level produced the best results, since SWT in combination with the NPs treatment led to a significative drop of HT-29 cells viability with respect to the healthy cells. This is particularly visible for the cells treated with 50 µg/mL L-ZnO or YSA-L-ZnO and 30 µg/mL YSA-L-ZnO. The latter case gave also prove of the enhanced effect of the targeting peptide on CRC cells, while 50 µg/mL dose ofYSA-L-ZnO is probably too high to appreciate the role of the peptide in the combined treatment. However, in general, L-ZnO produced less pronounced effects on CRC cells, which can be explained considering the lower internalization rates with respect to their targeted counterpart. These observations are supported by the calculations of synergy scores, obtained with SynergyFinder$^+$ (SynergyFinder—a FAIR tool for drug combination discovery; Ianevski et al. 2022), reported in Fig. 5B and C. A higher score indicates a synergistic effect (red),

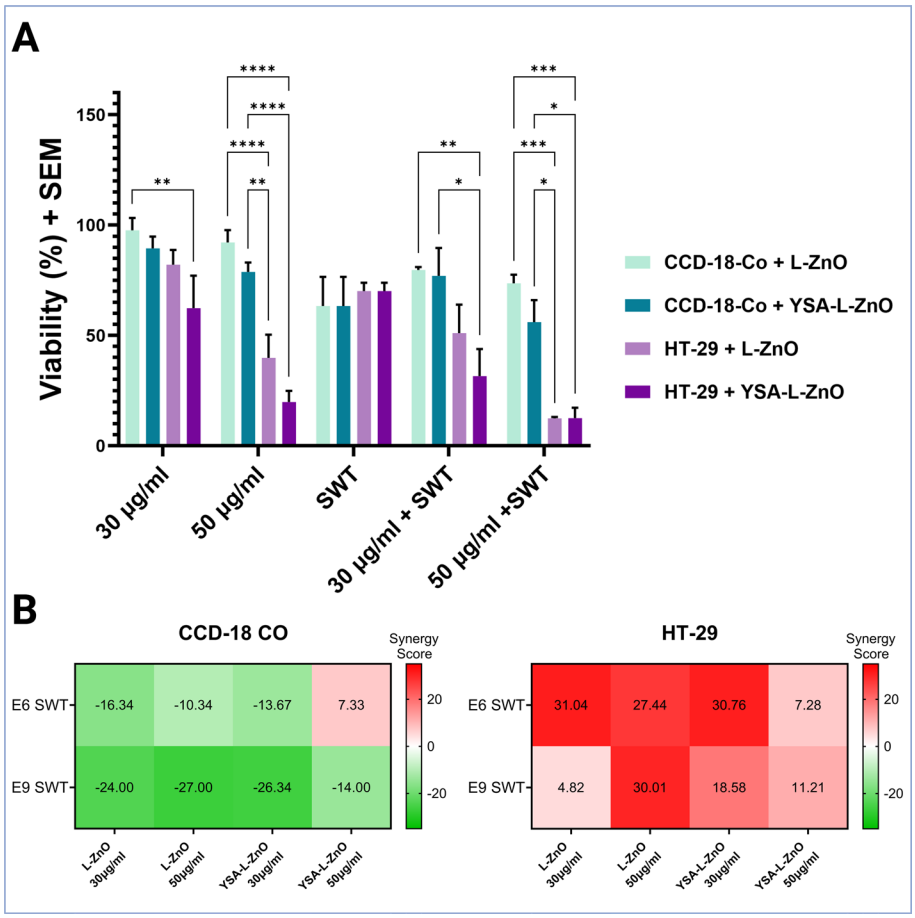

Fig. 5 **A** Combination treatment of CCD-18Co fibroblast-like, healthy colorectal cells and HT-29 CRC malignant cells cell cultures with L-ZnO or YSA-L-ZnO NPs and acoustic stimulation. Cells were seeded, left untreated or treated with L-ZnO or YSA-L-ZnO, at two different concentrations (30 and 50 µg/mL). After 24, 48 and 72 h, they were left untreated or subjected to a multiple shock wave Energy level E6, 0.22 mJ/mm^2. After 96 h from the NPs administration, cell viability was assessed. Data are expressed as normalized percentage with respect to the control sample, which was considered 100% viable. *$p < 0.0332$, **$p < 0.0021$, ***$p < 0.0002$, ****$p < 0.0001$. **B** Results of the synergy scores calculation of combination treatments, performed with SynergyFinder$^+$ (SynergyFinder—a FAIR tool for drug combination discovery) and visualized through synergy heatmaps on CCD-18Co and HT-29

while a lower one indicates an antagonistic effect (green); values between − 10 and 10 represent an additive interaction of the two treatments. It is in fact clear that the synergy scores were almost inexistent in CCD-18Co cell line, where antagonistic interactions were mostly found. In the CRC cell case, in contrast, several synergistic interactions were found, and the highest synergy scores were observed with E6 energy level, combined with both concentrations of L-ZnO or 30 µg/mL YSA-L-ZnO. Also E9 SWT with 50 µg/mL L-ZnO showed a particularly high synergy score, but in general, the synergy results obtained with E9 SWT were weaker than with E6. This can be justified considering that the highest energy level, as well as the highest YSA-L-ZnO dose, were already heavily impacting cell viability, making the synergistic action less evident.

Treatments in 3D spheroids

2D monolayer cultures were the first stage of this work, but such models, although very useful, show some important limitations in predicting the effectiveness of a treatment in the complex in vivo environment. With the aim to approach the complexity of a real CRC tumoral mass, the effects of lipid-coated ZnO and the SWT on HT-29 spheroids were tested.

3D cytotoxicity test

To assess the cytotoxicity of YSA-L-ZnO NPs and of the untargeted L-ZnO, spheroids were grown for 6 days. The 6th day after cell seeding, the NPs were administered and the spheroid viability was evaluated after 24, 48, 72 and 96 h, i.e. at days 7, 8, 9 and 10 (Fig. 1C). Remarkably, the only dose able to produce a statistically significant cytotoxicity in the cell spheroids was 100 μg/ml of YSA-L-ZnO NPs (Fig. 6A). Consequently, 3D spheroids demonstrated a higher resistance to NPs, with respect to 2D cell monolayer cultures. Our hypothesis is that the 3D structure of spheroids is more difficult to penetrate by the NPs than 2D monolayers due to their three-dimensional architecture. Here, despite the high number of cells, only the superficial layers of cells in the spheroid are directly exposed to NPs, probably, allowing a renewal of damaged cells from the spheroid core. In the 3D scenario, a targeting peptide can start to make the difference. In fact, a slight but consistent tendency of YSA-L-ZnO NPs to affect the spheroids more than L-ZnO is noticeable from 48 h after the treatment. To further confirm this hypothesis, a live-cell fluorescence microscopy experiment with calcein AM/PI dual staining was set up (Fig. 6B). At 24 and 48 h from YSA-L-ZnO NPs administration, a predominant green-fluorescent signal from viable cells is evident for all NPs doses. Also, a necrotic core, visible in the red channel, is slightly present in all cases and tends to intensify with the increase of NPs dose. As expected, the maximum red signal was obtained after 72 h post-administration, with the highest concentration of YSA-L-ZnO. These data visually confirm what already observed though flow cytometry and suggest that YSA-L-ZnO are able to impact on the core of spheroids, in a dose-dependent manner.

NPs uptake in 3D spheroids

In order to corroborate the role of YSA targeting peptide in the penetration of NPs in the spheroids volume, a 3D internalization test was set up. As previously done for the cytotoxicity assessment, fluorescently labelled particles were administered to the spheroids, which were then disaggregated and analysed through flow cytometry (Fig. 6C). Although no statistically significant difference between L-ZnO and YSA-L-ZnO was found, the tendency of the YSA-L-ZnO to be taken up more by CRC cells was consistently observed.

Stimuli-responsive combination treatment in 3D models

According to the scheme in Fig. 1C, HT-29 spheroids were treated with the combination L-ZnO or YSA-L-ZnO and repeated acoustic SWs.

After 24 h from the third SWT, the spheroids were disaggregated and analysed through flow cytometry. The data collected are presented in Fig. 7A. Also in this case, YSA-L-ZnO provoked more damages to CRC spheroids compared to the effect of untargeted

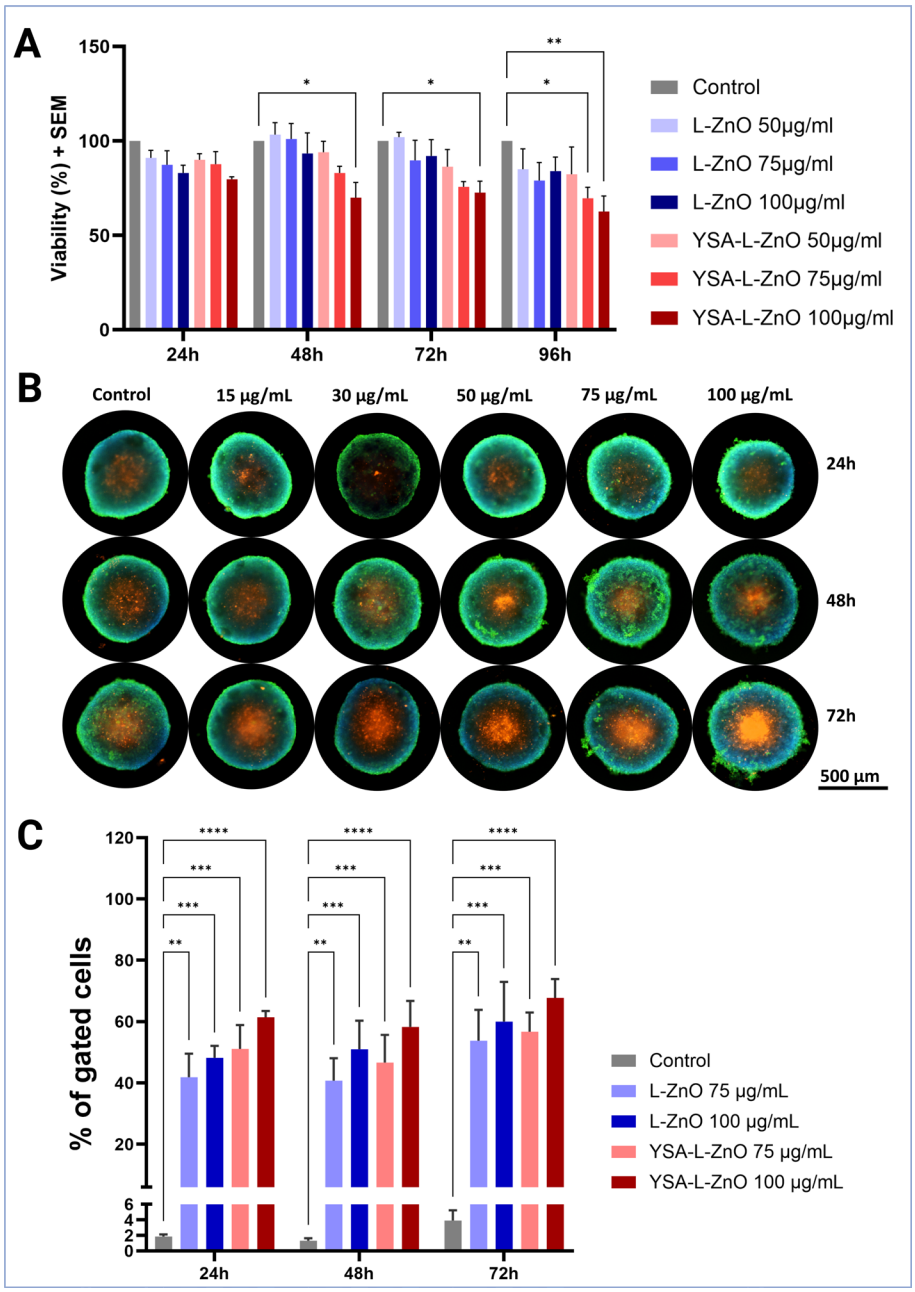

Fig. 6 **A** Cytotoxicity test of NPs on HT-29 spheroids. Spheroids were left untreated (control) or treated with different concentrations of targeted YSA-L-ZnO or with the untargeted control NPs (L-ZnO). After 24, 48, 72 and 96 h from the exposure, spheroids were disaggregated, dead cells were stained with propidium iodide, and the viability was measured through flow cytometry. Data are normalized by the control sample, which is considered to be 100% vital. **B** Live-cell fluorescence microscopy images of the spheroids treated with YSA-L-ZnO at different concentrations and time steps. Spheroids were stained with Calcein AM (green channel) and Propidium Iodide (red channel) to mark the live and the dead cells respectively; cell nuclei were also stained with Hoechst (blue channel). C) Flow cytometry results of internalization test on HT-29 spheroids. *$p < 0.0332$, **$p < 0.0021$, ***$p < 0.0002$, ****$p < 0.0001$

L-ZnO. Indeed, in the most stressful conditions, i.e. the combination of the highest dose of NPs together with SWs at the highest energy level (E9, 0.35 mJ/mm^2), YSA-L-ZnO considerably reduced the viability of the spheroid. Again, this can be attributed to the

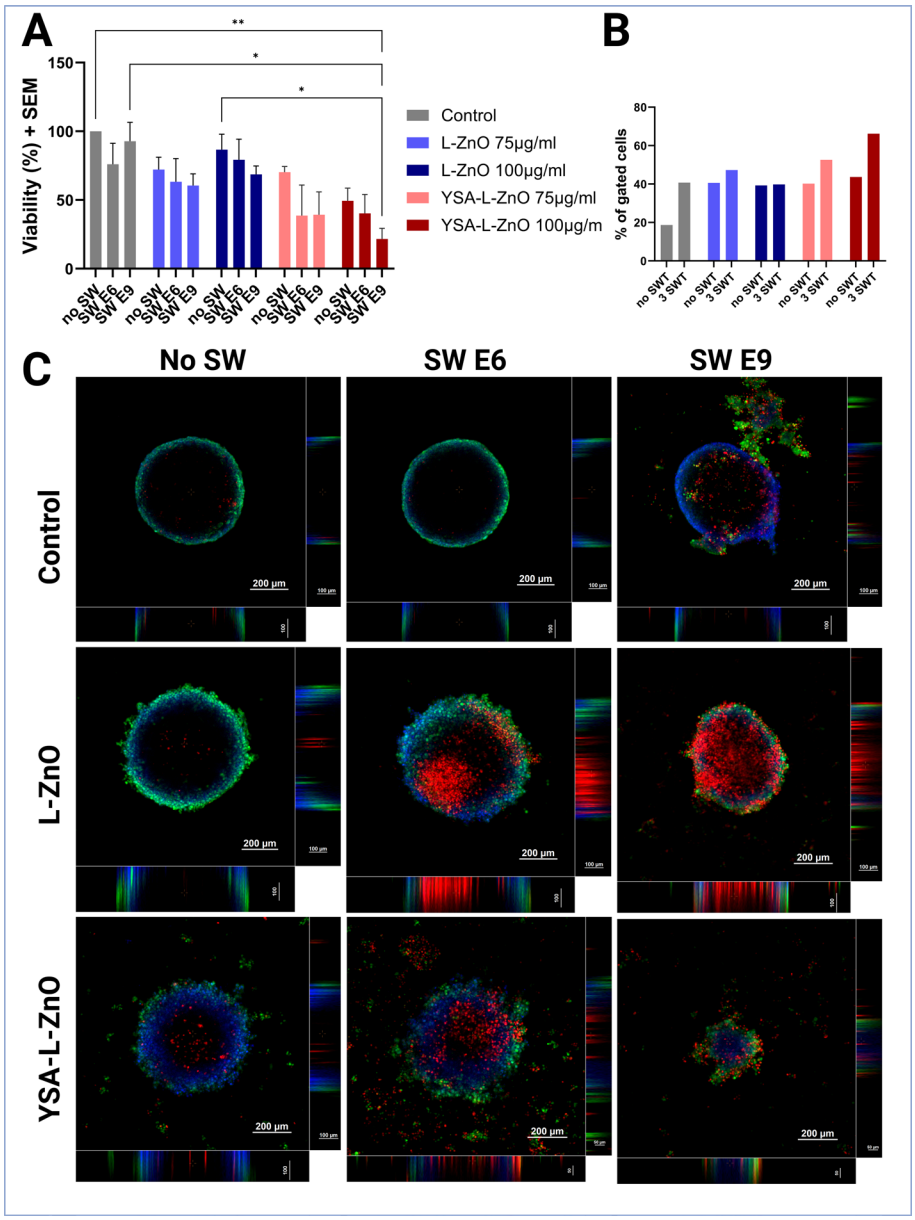

Fig. 7 Acoustic shock waves and YSA-L-ZnO NPs combination treatment in HT-29 cell spheroids. Spheroids were produced, grown for 5 days and left untreated (No NPs) or treated with nanoparticles (YSA-L-ZnO NPs or with the non-targeted L-ZnO NPs as control, both at 100 µg/mL), testing two different concentrations. After 24, 48 and 72 h, spheroids were either subjected to a multiple shock wave (SW) treatment at two different SW intensities (Energy level E6, 0.22 mJ/mm^2 and energy level E9, 0.35 mJ/mm^2) or not (no SW). A) After 96 h from the administration of the nanoparticles, cell viability was assessed through flow cytometry, by spheroid disaggregation. Data are normalized by the control sample, which is considered to be 100% vital. *$p < 0.0332$, **$p < 0.0021$, ***$p < 0.0002$, ****$p < 0.0001$. B) Results of evaluation of apoptosis levels through Annexin V assay under flow cytometry. 100 µg/mL L-ZnO and YSA-L-ZnO were administered to spheroids and the analyses were performed after a triple SW treatment at E9 energy level C) Fluorescence microscopy images after the second SW stimulation (48 h time step) combined with L-ZnO or YSA-L-ZnO. Both slices and lateral projections from Z-stacks are presented. Spheroids were stained with Calcein AM (green) and PI (red) to mark live and dead cells, respectively; cell nuclei were also stained with Hoechst (blue)

higher capability of YSA-L-ZnO to penetrate the spheroids, conferred by the targeting ligand. Remarkably, the control experiment adopting untargeted L-ZnO NPs revealed almost unaffected spheroids after the combination treatment. Furthermore, individual treatments of SWs and NPs at the 75 μg/mL dose were proven to be ineffective. This corroborates what discussed above, confirming that spheroids tolerate higher doses of NPs with respect to their 2D monolayers counterparts, probably due to their 3D organization. As in the 2D treatment experiment, the combined action of SWs and the highest dose of YSA-L-ZnO NPs led to the highest mortality of cells and the most statistically significant data, confirming the efficacy of such treatment also in the complex 3D environment. The synergy between NPs and SWT is reported in Figure S6 of the S.I.: although some synergy was found in L-ZnO-treated samples, the highest synergy scores were reached in spheroids treated with YSA-L-ZnO and with both SW energy levels, attesting the synergistic action of the targeted nanoconstruct and the remote stimulation.

In search for clues about the mechanism of death triggered by the SWT, the levels of Annexin V apoptotic marker were evaluated in spheroids after the combined treatment by flow cytometry. The results after a single SWT or a triple SWT (3 SWT) are presented in Figure S7 and Fig. 7B, respectively. From these data it is evident that SWs are able to induce an apoptotic pathway in CRC cells. Moreover, from Fig. 7B, it is visible that YSA-L-ZnO, together with 3 SWT, produced the highest apoptotic signal, attesting the percentage of apoptotic cells above 60%, while the other treatments were unable to overcome 45%, confirming the previous findings.

Finally, fluorescence microscopy was adopted to have a qualitative insight of the spheroid viability during the combined treatment. Figure 7C collects the z-stack images taken after the second SW treatment which represents the most significant results, while the complete set of images after each SWT can be found in the S.I. (Figures S8 and S9 of the S.I.). The spheroids treated with YSA-L-ZnO NPs and SWT are subjected to a drastic reduction of the dimensions, mostly appreciable for the 48 h and 72 h time-steps. Over time, we assist to the disintegration of the spheroids treated with YSA-L-ZnO and E9 SW, which leads to the almost complete extinction of the spheroid mass in the last two time-steps (bottom right panels in Fig. 7C and Figure S9). The absence of a strong PI signal in these samples can be justified considering that the high-energy of the used SWs, in combination with YSA-L-ZnO, could be strong enough to quickly and completely destroy cells. The red signal of the PI is clearly visible in the samples treated with L-ZnO NPs and SWT, as red areas inside the spheroids. These red areas are wider and deeper in the spheroid treated with L-ZnO and E9 SW, attesting the SW energy-dependent cellular damage leading to suffering cells. On the other hand, SWT alone (first row in Fig. 7C and Figures S8 and S9 of the S.I.) seems to have a weak effect on the spheroids, and even the highest SW energy appears to undermine more the integrity of the 3D structure, rather than the cell viability of the spheroids (see pictures in the first raw and right column in Fig. 7C and Figure S9 of the S.I.).

Conclusions

In view of the recent and most exciting advances in nanomedicine, it is proposed the formulation of biomimetic core–shell nanoparticles for synergistic cancer treatment with acoustic pressure waves, here applied to 3D tumor models of colorectal cancer. These

NPs have indeed a protective and biomimetic shell, a targeting peptide for colon cancer selectivity, and an inorganic core consisting in iron-doped zinc oxide nanocrystals.

This work proposed an innovative stimuli-responsive therapy based on the activation of these hybrid and targeted nanoparticles by acoustic pressure stimulation, i.e. high-pressure shock waves, able to act in deep-seated tumors and allowing the generation of mechanical damages to cells and cytotoxic responses leading to cell apoptosis.

These hybrid nanoparticles were proven to be per se highly biocompatible, hemocompatible and minimally toxic for healthy cells, even at the highest tested doses. On the contrary, cancerous colorectal cells were found sensitive to high doses of NPs, in particular the targeted ones, being efficiently internalized in the tumor cells while sparing the healthy counterpart. Synergistic effects were observed in 3D colorectal cancer spheroid models, where the combination of targeted nanoparticles and repeated acoustic stimulations led, at the highest doses, to the complete ablation of CRC mass. Altogether, these findings pave the way for further pre-clinical and clinical validations of this remotely-controlled nanomedicine approach.

Supplementary Information

The online version contains supplementary material available at https://doi.org/10.1186/s12645-024-00281-3.

Additional file 1.

Acknowledgements
The authors wish also to thank the company ELvation Medical GmbH for providing the instrument PiezoWave2 from Richard Wolf.

Author contributions
G.R. carried out the main experiments, prepared all figures and wrote the main manuscript; G.M., B.D., M.C (Carofiglio), M.C. (Conte) set up the methodology, contributed to the experimental validation and to the results discussion; A.G. contributed to the experimental validation and with funding; G.M., B.D. and V.C. supervised, V.C. contributed with funding and project management. All authors reviewed the manuscript.

Funding
This work has received funding from the European Union's Horizon 2020 Research and Innovation program under Grant agreement No 964386—FET Open RIA project acronym "MimicKEY", from the European Research Council (ERC) under Grant agreement No. 957563—Project Acronym "XtraUS"—ERC Proof of Concept Grant, from the National Plan for Complementary Investments to the NRRP, project "D34H—Digital Driven Diagnostics, prognostics and therapeutics for sustainable Health care" (project code: PNC0000001), Spoke 4 funded by the Italian Ministry of University and Research, and from the Nancy Owen's Breast Cancer Foundation.

Data availability
Data is provided within the manuscript or supplementary information files.

Declarations

Conflict of interest
The authors declare no competing interests.

Received: 25 May 2024 Accepted: 27 July 2024
Published online: 08 August 2024

References

Barui S, Percivalle NM, Conte M et al (2022) Development of doped ZnO-based biomimicking and tumor-targeted nanotheranostics to improve pancreatic cancer treatment. Cancer Nanotechnol 13:1–24. https://doi.org/10.1186/S12645-022-00140-Z/FIGURES/11

Barui S, Conte M, Percivalle NM et al (2023) Dual drug loaded nanotheranostic platforms as a novel synergistic approach to improve pancreatic cancer treatment. Part Part Syst Charact 40:2200138. https://doi.org/10.1002/PPSC.202200138

Bisht G, Rayamajhi S (2016) ZnO nanoparticles: a promising anticancer agent. Nanobiomedicine (rij). https://doi.org/10.5772/63437
Breslin S, O'Driscoll L (2013) Three-dimensional cell culture: the missing link in drug discovery. Drug Discov Today 18:240–249. https://doi.org/10.1016/J.DRUDIS.2012.10.003
Canavese G, Ancona A, Racca L et al (2018) Nanoparticle-assisted ultrasound: a special focus on sonodynamic therapy against cancer. Chem Eng J 340:155–172. https://doi.org/10.1016/J.CEJ.2018.01.060
Canta M, Cauda V (2020) The investigation of the parameters affecting the ZnO nanoparticle cytotoxicity behaviour: a tutorial review. Biomater Sci 8:6157–6174. https://doi.org/10.1039/D0BM01086C
Carofiglio M, Barui S, Cauda V, Laurenti M (2020) Doped zinc oxide nanoparticles: synthesis, characterization and potential use in nanomedicine. Appl Sci 10:5194. https://doi.org/10.3390/APP10155194
Carofiglio M, Laurenti M, Vighetto V et al (2021) Iron-doped zno nanoparticles as multifunctional nanoplatforms for theranostics. Nanomaterials 11:2628. https://doi.org/10.3390/NANO11102628/S1
Carofiglio M, Conte M, Racca L, Cauda V (2022) Synergistic phenomena between iron-doped ZnO nanoparticles and shock waves exploited against pancreatic cancer cells. ACS Appl Nano Mater 5:17212–17225. https://doi.org/10.1021/ACSANM.2C04211/ASSET/IMAGES/LARGE/AN2C04211_0010.JPEG
Cauda V, Engelke H, Sauer A et al (2010) Colchicine-loaded lipid bilayer-coated 50 nm mesoporous nanoparticles efficiently induce microtubule depolymerization upon cell uptake. Nano Lett 10:2484–2492. https://doi.org/10.1021/NL100991W
Cauda V, Xu TT, Nunes I et al (2021) Biomimetic mesoporous vectors enabling the efficient inhibition of wild-type isocitrate dehydrogenase in multiple myeloma cells. Microporous Mesoporous Mater 325:111320. https://doi.org/10.1016/J.MICROMESO.2021.111320
Conte M, Carofiglio M, Rosso G, Cauda V (2023) Lipidic formulations inspired by COVID vaccines as smart coatings to enhance nanoparticle-based cancer therapy. Nanomaterials. https://doi.org/10.3390/NANO13152250
Costa EC, Moreira AF, de Melo-Diogo D et al (2016) 3D tumor spheroids: an overview on the tools and techniques used for their analysis. Biotechnol Adv 34:1427–1441. https://doi.org/10.1016/J.BIOTECHADV.2016.11.002
Danaei M, Dehghankhold M, Ataei S et al (2018) Impact of particle size and polydispersity index on the clinical applications of lipidic nanocarrier systems. Pharmaceutics. https://doi.org/10.3390/PHARMACEUTICS10020057
Deng B, Liu S, Wang Y et al (2024) Oral nanomedicine: challenges and opportunities. Adv Mater 36:1–22. https://doi.org/10.1002/adma.202306081
Dumontel B, Canta M, Engelke H et al (2017) Enhanced biostability and cellular uptake of zinc oxide nanocrystals shielded with a phospholipid bilayer. J Mater Chem B 5:8799–8813. https://doi.org/10.1039/c7tb02229h
European Medicines Agency (2021) EMA implements new measures to minimise animal testing during medicines development
Foglietta F, Serpe L, Canaparo R (2021) The effective combination between 3D cancer models and stimuli-responsive nanoscale drug delivery systems. Cells. https://doi.org/10.3390/CELLS10123295
George S, Pokhrel S, Xia T et al (2010) Use of a rapid cytotoxicity screening approach to engineer a safer zinc oxide nanoparticle through iron doping. ACS Nano 4:15–29. https://doi.org/10.1021/NN901503Q
Han JJ (2023) FDA Modernization Act 2.0 allows for alternatives to animal testing. Artif Organs 47:449–450. https://doi.org/10.1111/AOR.14503
Ianevski A, Giri AK, Aittokallio T (2022) SynergyFinder 3.0: an interactive analysis and consensus interpretation of multi-drug synergies across multiple samples. Nucleic Acids Res 50:W739–W743. https://doi.org/10.1093/NAR/GKAC382
Koolpe M, Dail M, Pasquale EB (2002) An ephrin mimetic peptide that selectively targets the EphA2 receptor. J Biol Chem 277:46974–46979. https://doi.org/10.1074/JBC.M208495200
Leenhardt R, Camus M, Mestas JL et al (2019) Ultrasound-induced cavitation enhances the efficacy of chemotherapy in a 3D model of pancreatic ductal adenocarcinoma with its microenvironment. Sci Rep 9:18916–18916. https://doi.org/10.1038/S41598-019-55388-0
Li B, Wang F, Gui L et al (2018) The potential of biomimetic nanoparticles for tumor-targeted drug delivery. Nanomedicine (london) 13:2099–2118. https://doi.org/10.2217/NNM-2018-0017
Li Y, Hao L, Liu F et al (2019) Cell penetrating peptide-modified nanoparticles for tumor targeted imaging and synergistic effect of sonodynamic/HIFU therapy. Int J Nanomedicine 14:5875–5894. https://doi.org/10.2147/IJN.S212184
Luchini A, Vitiello G (2019) Understanding the nano-bio interfaces: lipid-coatings for inorganic nanoparticles as promising strategy for biomedical applications. Front Chem 7:343. https://doi.org/10.3389/FCHEM.2019.00343
Morris VK, Kennedy EB, Baxter NN et al (2023) Treatment of metastatic colorectal cancer: ASCO guideline. J Clin Oncol 41:678–700. https://doi.org/10.1200/JCO.22.01690
Ouyang J, Deng B, Zou B et al (2023a) Oral hydrogel microbeads-mediated in situ synthesis of selenoproteins for regulating intestinal immunity and microbiota. J Am Chem Soc 145:12193–12205. https://doi.org/10.1021/jacs.3c02179
Ouyang J, Zhang Z, Deng B et al (2023b) Oral drug delivery platforms for biomedical applications. Mater Today 62:296–326. https://doi.org/10.1016/J.MATTOD.2023.01.002
Ozsoy F, Mohammed M, Jan N et al (2024) T cell and natural killer cell membrane-camouflaged nanoparticles for cancer and viral therapies. ACS Appl Bio Mater 7:2637–2659. https://doi.org/10.1021/ACSABM.4C00074/ASSET/IMAGES/LARGE/MT4C00074_0013.JPEG
Percivalle NM, Carofiglio M, Conte M et al (2022) Artificial and naturally derived phospholipidic bilayers as smart coatings of solid-state nanoparticles: current works and perspectives in cancer therapy. Int J Mol Sci 23:15815. https://doi.org/10.3390/IJMS232415815
Prasad R, Mendes BB, Gorain M et al (2023) Bioinspired and biomimetic cancer-cell-derived membrane nanovesicles for preclinical tumor-targeted nanotheranostics. Cell Rep Phys Sci. https://doi.org/10.1016/J.XCRP.2023.101648
Prasad R, Jyothi VGS, Kommineni N et al (2024a) Biomimetic ghost nanomedicine-based optotheranostics for cancer. Nano Lett. https://doi.org/10.1021/ACS.NANOLETT.4C01534
Prasad R, Peng B, Mendes BB et al (2024b) Biomimetic bright optotheranostics for metastasis monitoring and multimodal image-guided breast cancer therapeutics. J Control Release 367:300–315. https://doi.org/10.1016/j.jconrel.2024.01.056

Racca L, Rosso G, Carofiglio M et al (2023) Effective combination of biocompatible zinc oxide nanocrystals and high-energy shock waves for the treatment of colorectal cancer. Cancer Nanotechnol 14:1–21. https://doi.org/10.1186/S12645-023-00195-6/FIGURES/8
Rosso G, Cauda V (2023) Biomimicking extracellular vesicles with fully artificial ones: a rational design of EV-BIOMIMETICS toward effective theranostic tools in nanomedicine. ACS Biomater Sci Eng 9:5924–5932. https://doi.org/10.1021/ACSBIOMATERIALS.2C01025
Roy M, Alix C, Bouakaz A et al (2023) Tumor spheroids as model to design acoustically mediated drug therapies: a review. Pharmaceutics 15:806. https://doi.org/10.3390/PHARMACEUTICS15030806
Sabu C, Rejo C, Kotta S, Pramod K (2018) Bioinspired and biomimetic systems for advanced drug and gene delivery. J Control Release 287:142–155. https://doi.org/10.1016/J.JCONREL.2018.08.033
Schnorenberg MR, Yoo SP, Tirrell MV, Labelle JL (2018) Synthesis and purification of homogeneous lipid-based peptide nanocarriers by overcoming phospholipid ester hydrolysis. ACS Omega 3:14144–14150. https://doi.org/10.1021/ACSOMEGA.8B01772
Searson PC (2023) The Cancer Moonshot, the role of in vitro models, model accuracy, and the need for validation. Nat Nanotechnol 18:1121–1123. https://doi.org/10.1038/s41565-023-01486-0
Shin AE, Giancotti FG, Rustgi AK (2023) Metastatic colorectal cancer: mechanisms and emerging therapeutics. Trends Pharmacol Sci 44:222–236. https://doi.org/10.1016/J.TIPS.2023.01.003
Sun L, Ke J, He Z et al (2017) HES1 promotes colorectal cancer cell resistance to 5-Fu by inducing of EMT and ABC transporter proteins. J Cancer 8:2802. https://doi.org/10.7150/JCA.19142
Sung H, Ferlay J, Siegel RL et al (2021) Global Cancer Statistics 2020: GLOBOCAN Estimates of Incidence and Mortality Worldwide for 36 Cancers in 185 Countries. CA Cancer J Clin 71:209–249. https://doi.org/10.3322/caac.21660
Tavano R, Segat D, Reddi E et al (2010) Procoagulant properties of bare and highly PEGylated vinyl-modified silica nanoparticles. Nanomedicine (london) 5:881–896. https://doi.org/10.2217/NNM.10.65
Tchoryk A, Taresco V, Argent RH et al (2019) Penetration and uptake of nanoparticles in 3D tumor spheroids. Bioconjug Chem 30:1371–1384. https://doi.org/10.1021/ACS.BIOCONJCHEM.9B00136
Tian L, Pei R, Zhong L et al (2021) Enhanced targeting of 3D pancreatic cancer spheroids by aptamer-conjugated polymeric micelles with deep tumor penetration. Eur J Pharmacol 894:173814. https://doi.org/10.1016/j.ejphar.2020.173814
Vakhshiteh F, Bagheri Z, Soleimani M et al (2023) Heterotypic tumor spheroids: a platform for nanomedicine evaluation. J Nanobiotechnol 21:1–33. https://doi.org/10.1186/S12951-023-02021-Y
Wang L, Li G, Cao L et al (2021) An ultrasound-driven immune-boosting molecular machine for systemic tumor suppression. Sci Adv. https://doi.org/10.1126/SCIADV.ABJ4796
Weiswald LB, Bellet D, Dangles-Marie V (2015) Spherical cancer models in tumor biology. Neoplasia 17:1–15. https://doi.org/10.1016/J.NEO.2014.12.004
Xia T, Zhao Y, Sager T et al (2011) Decreased dissolution of ZnO by iron doping yields nanoparticles with reduced toxicity in the rodent lung and zebrafish embryos. ACS Nano 5:1223–1235. https://doi.org/10.1021/NN1028482/SUPPL_FILE/NN1028482_SI_002.PDF
Xie YH, Chen YX, Fang JY (2020) Comprehensive review of targeted therapy for colorectal cancer. Signal Transduct Target Ther 5:22. https://doi.org/10.1038/s41392-020-0116-z
Zanoni M, Piccinini F, Arienti C et al (2016) 3D tumor spheroid models for in vitro therapeutic screening: a systematic approach to enhance the biological relevance of data obtained. Sci Rep 6:1–11. https://doi.org/10.1038/srep19103
Zhang L, Song R, Gu D et al (2017) The role of GLI1 for 5-Fu resistance in colorectal cancer. Cell Biosci 7:17. https://doi.org/10.1186/S13578-017-0145-7
Zhang F, Xin C, Dai Z et al (2022) Oncocyte membrane-camouflaged multi-stimuli-responsive nanohybrids for synergistic amplification of tumor oxidative stresses and photothermal enhanced cancer therapy. ACS Appl Mater Interfaces 14:40633–40644. https://doi.org/10.1021/ACSAMI.2C11200
Zhang P, Zhu F, Long H et al (2023) Study of the mechanism of ultrasound-induced enhanced therapeutic effects of a chitosan-based nanoplatform. Biomed Mater 18:045030. https://doi.org/10.1088/1748-605X/ACE018

Publisher's Note